Двенадцатая Международная научно-техническая конференция
«Оптические методы исследования потоков»
Москва, 25 — 28 июня 2013 г.

УДК 533.6.08

Laboratory and flight tests of IPCT method

F.Boden[1], A.Yu. Poroykov[2], B.S. Rinkevichyus[2], N.M. Skornyakova[2]

[1]DLR, [2]National Research University “MPEI”

ANNOTATION

The investigations of the theoretically and in the laboratory experiment of Image Pattern Correlation Technique are presented in this paper. The dependence of the effect of the viewing angle on the results obtained. The possibility of IPCT applying for flight testing given.

IMAGE PATTERN CORRELATION TECHNIQUE, IN-FLIGHT MEASUREMENTS, DYNAMIC DEFORMATION

INTRODUCTION

Image Pattern Correlation Technique (IPCT) is high precision optical measurement of surface shape and surface deformation which is based on computer processing of images with the help of correlation algorithms. It also can be applied for controlling surface movement and rotation. For deformation analysis areas on the test object which are suspected to suffer deformation are covered with special image – pattern (background screen). Pattern can be a random dot image or something else. After deformation surface of test object changing and images of pattern which is getting with the help of camera before and after deformation differ. So after processing these images information about test object deformation can be obtained. Cross correlation processing consist in dividing two images into small parts and calculating function of correlations of corresponding parts. Maximum of correlating function shows us direction and amount of image part displacement. Special mathematical model allow to make qualitative or quantitative vector field of deformation (displacement) using information of displacements [1 – 3].

1. THEORETICAL INVESTIGATION

For successfully applying IPCT for in-flight full-scale tests, limits of possibilities for this technique appearing in case of arrangement of the investigation surface and measures which can reduce these limitations must be defined. In order to define in what way large angle between the image plane and investigating plane effects on experimental results, a mathematical model of image formation must be created. Well known that an image formation in optical systems is done via the perspective projection. [4] The scheme of such a projection is shown in Figure 1.

The observation point B is projected into the image point E. Zero of camera coordinate system is located at the point O (the center of the optical system). Line FA is the optical axis of the system. It crosses the rear image plane, the front image plane and object plane at the points F, C and A, respectively. Coordinate of point B in a coordinate system of object plane is x_c. Coordinate of point E in the camera coordinate system is x_i. Distance from the center of the optical system to the

object plane is equal z_c. Focal length of optical system is f. Point D is the projection of point B on the front image plane.

As triangles OFE and OAB is similar, next formula can be written

$$\frac{x_i}{f} = \frac{x_c}{z_c}. \tag{1}$$

Thus, the actual coordinate of point E on the two-dimensional image is a spatial coordinate of point B, taken at a scale equal to the ratio of focal distance and the distance to the object.

For further mathematical model creating it will be convenient to consider the formation of the image not in the rear image plane, which is located behind the optical system, but in front image plane. From the similarity of triangles OFE and OCD can be written

$$\frac{x_f}{f} = \frac{x_c}{z_c}. \tag{2}$$

From formula (2) is clear that the dimensions of objects in these two planes will coincide, but in front image plane, they will not be mirrored with respect to real objects.

Figure 1 shows the simplest scheme perspective projection in which the investigation surface parallel to the image plane and the projection with respect to only one coordinate is considered. As mentioned above, in full-scale experiments this scheme can not be used. In most cases the investigation surface, which can be propeller blade or a wing, is situated at some angle to the image plane. It is therefore necessary to consider a more complex scheme of the perspective projection. Such scheme is shown in Figure 2.

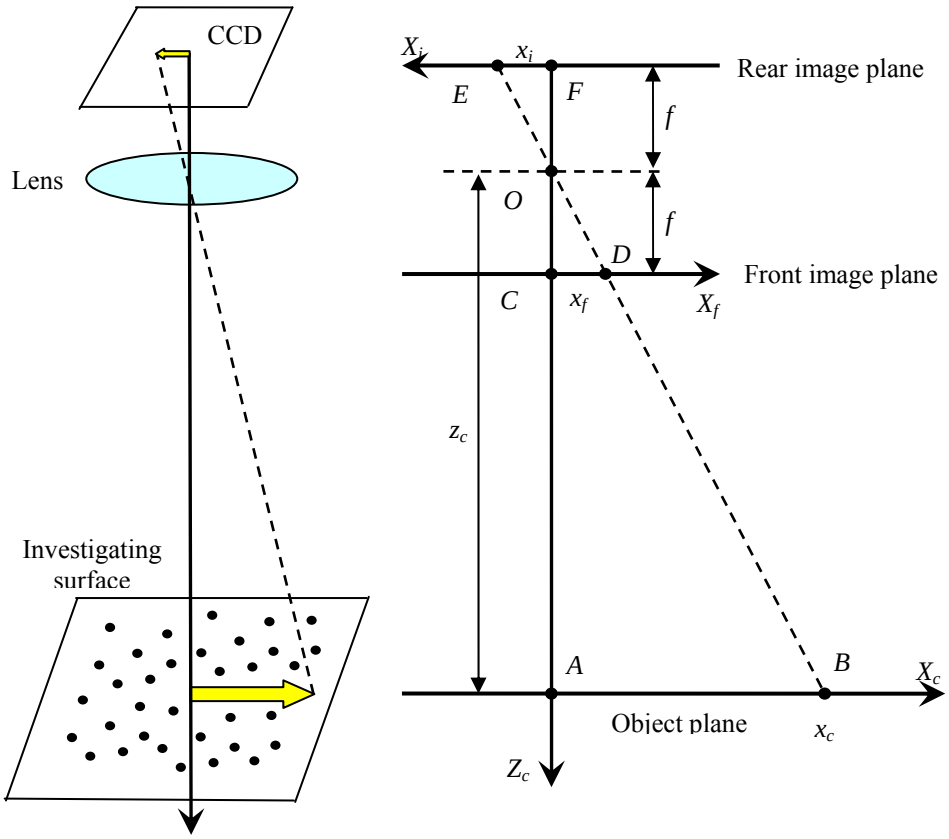

Figure 1 – Geometric scheme of perspective projection in optical system

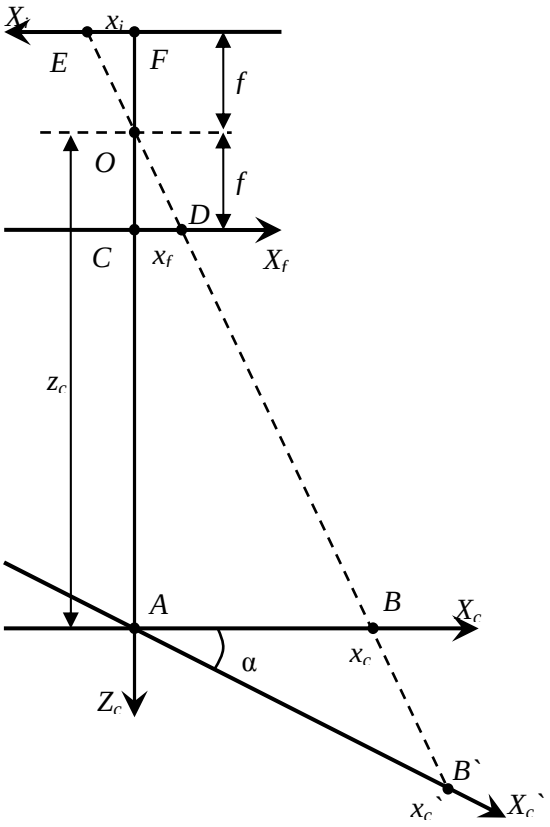

Figure 2 – Geometric scheme of perspective projection with non parallel investigation surface and image plane

In this new scheme, an additional axis $AX_c`$ that corresponds to the investigation surface inclined at an angle α to the image plane added. The point under consideration on the investigation surface is at point B`.

Like in the first scheme point B` is projected at point E on the rear image plane and at the point D on the front image plane. However, in the coordinate system of investigation surface it has a coordinate $x_c`$, which does not coincide with the coordinate x_c.

In order to link the coordinates of point B` with the coordinate of the point E additional plotting, which are shown in Figure 3, must be done. As can be seen from this figure, the optical axis was used to construct a right triangle AA`B`. Angle BAB` and the angle AB`A` are equal. So we can written the length of the cathetus AA` as

$$\Delta z_c = x_c^{'} \sin\alpha . \tag{3}$$

Similar, the length of cathetus A`B` can be written

$$x_c^{''} = x_c^{'} \cos\alpha . \tag{4}$$

Now, similarly to formula (1) the expression for the triangle OFE and completed the triangle OA`B`` can be written

$$\frac{x_i}{f} = \frac{x_c^{''}}{z_c + \Delta z_c}, \tag{5}$$

substituting in (5) (4) and (3) we obtain the expression

$$\frac{x_i}{f} = \frac{x_c^{'} \cos\alpha}{z_c + x_c^{'} \sin\alpha}. \qquad (6)$$

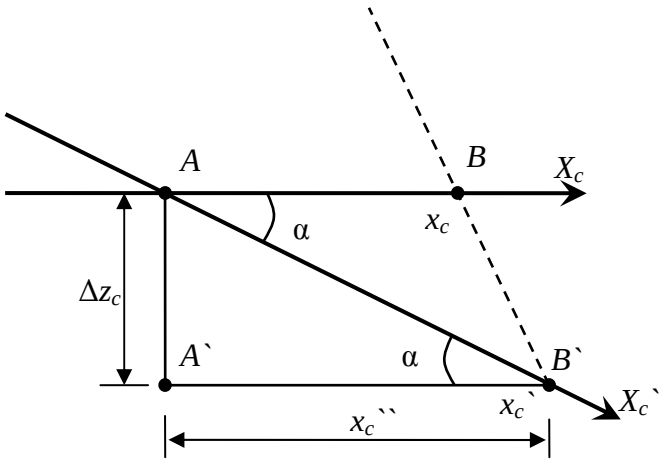

Figure 3 – Additional plotting for linking point B` coordinates in the investigation surface with coordinates of the point E on the image plane

Transforming formula (6) the final formula linking the coordinates of points on the investigation surface with the coordinates of points on the image plane in the projective projection can be obtained

$$x_i = \frac{x_c^{'} f \cos\alpha}{z_c + x_c^{'} \sin\alpha}. \qquad (7)$$

Using last expression curves of points coordinates in the image plane dependence on points coordinates on the investigation surface can be plotted (Figure 4). These curves show that when the angle between the image plane and the investigation plane is zero ($\alpha = 0$), the dependence is linear. This case corresponds to the perspective projection, which is shown in Figure 1. It is also possible to show from formula (7), which in case of $\alpha = 0$ is substituting into a formula (1).

When the angle between the image plane and the investigation surface is equal to 30° ($\alpha = 30°$), the dependence is seemed more complicated then in zero case, and it is not symmetric about the optical axis. With increasing angle α to 80° dependence becomes less steep. In the extreme case when the angle α is equal to 90 °, the dependence will be a horizontal line.

Plotted dependence makes mention two problems that arise when the investigation surface is arranged at large angle. The first of the problems is the nonlinear dependence of the coordinates of pixels on the coordinates of the points of the surface. Thus, to obtain reliable results of measurement and error reduction is necessary to make the calibration procedure and further de-warp of the original image to prevent nonlinearities. The second problem relates to the limitation of spatial resolution of images at high angle α.

Consider the dependence of the spatial resolution of images on the angle between the image plane and the investigation surface. The spatial resolution depends on the size of the CCD or CMOS and the pixel size of this sensor. For calculating spatial resolution of the image the length of the

image space that corresponds to the unit of the length in the objective space must be defined. For this, we differentiate expression (7) by x_c'

$$\frac{dx_i}{dx_c} = \frac{f\cos\alpha}{z_c + x_c'\sin\alpha} - \frac{x_c' f\sin\alpha\cos\alpha}{\left(z_c + x_c'\sin\alpha\right)^2}. \qquad (8)$$

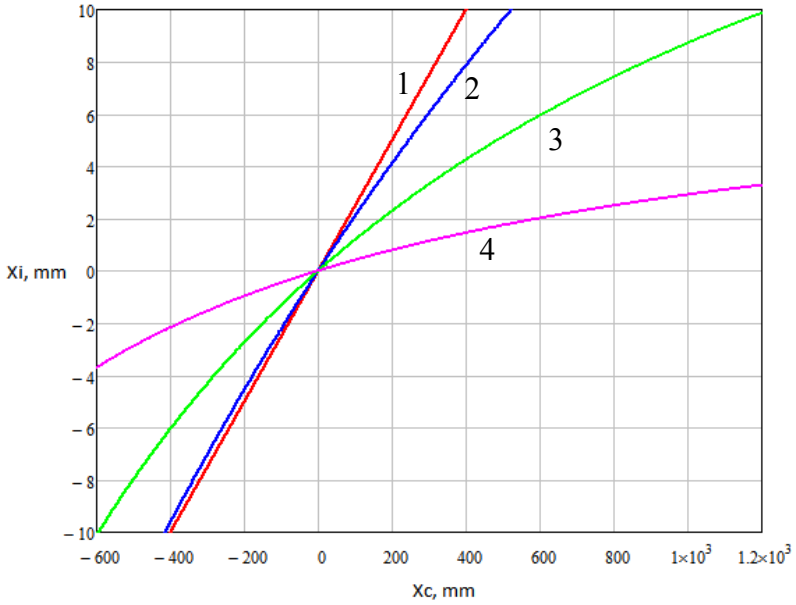

1 – $\alpha = 0$, 2 – $\alpha = 30°$, 3 – $\alpha = 60°$, 4 – $\alpha = 80°$

Figure 4 – Curves of points E coordinates in the image plane dependence on points B` coordinates on the investigation surface ($f = 50$ мм, $z_c = 2$ м)

Now, dividing the resulting expression on the size of one pixel of the CCD or CMOS, an expression for the spatial resolution of image can be obtained

$$S = \frac{1}{a}\left[\frac{f\cos\alpha}{z_c + x_c'\sin\alpha} - \frac{x_c' f\sin\alpha\cos\alpha}{\left(z_c + x_c'\sin\alpha\right)^2}\right], \qquad (9)$$

where S – is a spatial resolution of the image, and a – is dimension of the CCD or CMOS sensors pixel.

Using formula (9) the dependence of spatial resolution of image on the angle between the image plane and the investigation surface can be plotted (Figure 5).

Figure 5 shows that the dependence is nonlinear and is significantly differ for different coordinates x_c'. At a zero angle of α sensitivity is the same for all values of coordinates x_c' because the investigating surface is parallel to the image plane. As the angle α increasing points with negative coordinates, which corresponds to the part of investigation surface, which is closer to the lens, get greater spatial resolution.

For points located in the positive area on the contrary the resolution decreased. This is explained by the fact that at the same coordinate x_c' value increasing the angle α removing points farther from the lens.

Similarly, the dependence of spatial resolution of images on the coordinates of a point can be plotted (Figure 6).

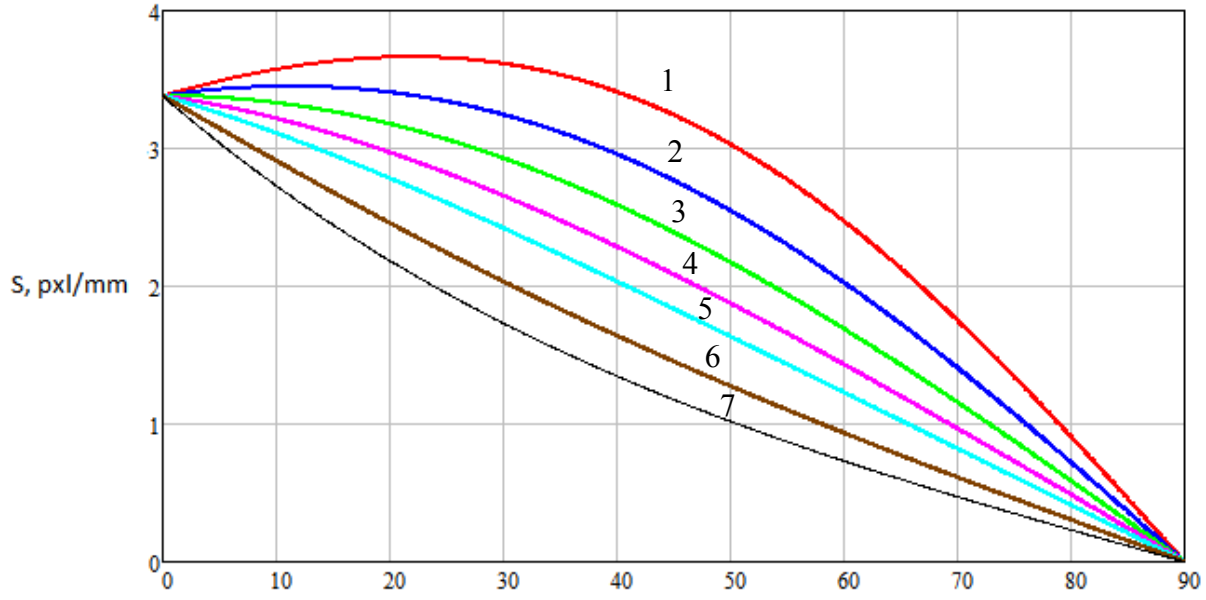

1 – x_c' = –400 mm, 2 – x_c' = –200 mm, 3 – x_c' = 0 mm,
4 – x_c' = 200 mm, 5 – x_c' = 400 mm, 6 – x_c'' = 800 mm, 7 – x_c' = 1200 mm

Figure 5 – Dependence of spatial resolution of images on angle between the investigating surface and the image plane (f = 50 mm, z_c = 2 m, a = 7,4 μm)

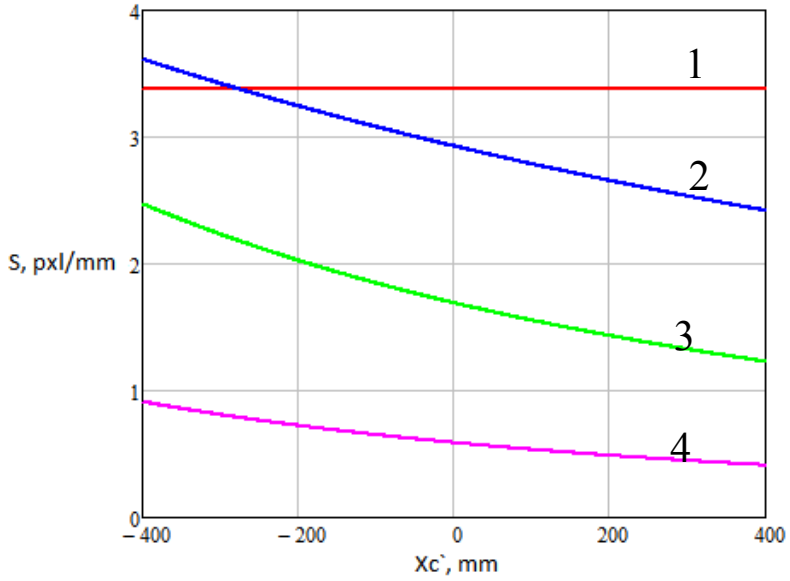

1 – α = 0, 2 – α = 30°, 3 – α = 60°, 4 – α = 80°

Figure 6 – Dependence of spatial resolution of images on the coordinates of a point on the investigating surface (f = 50 mm, z_c = 2 m, a = 7,4 μm)

Dependence of spatial resolution of images on the distance to the image plane is plotted on Figure 7.

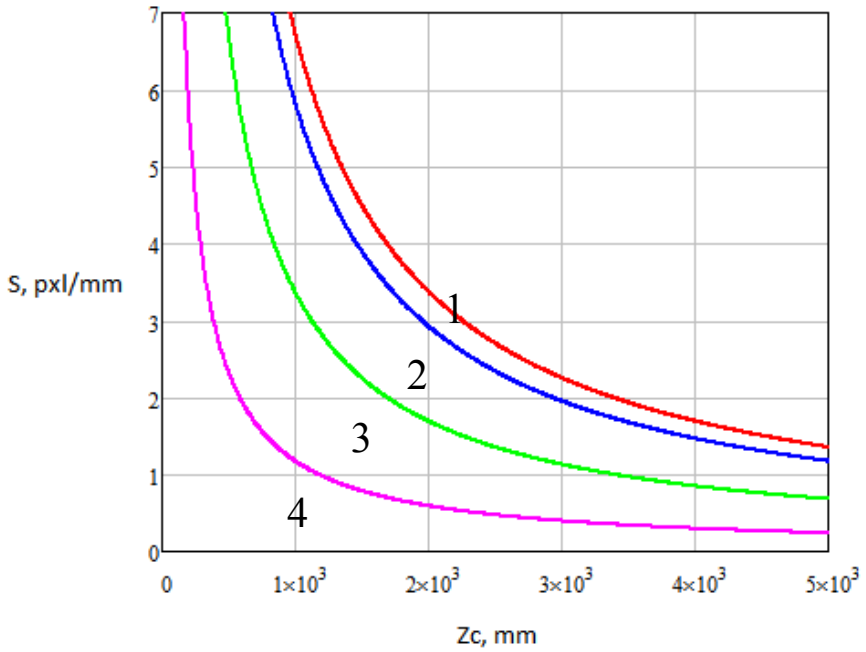

1 – $\alpha = 0$, 2 – $\alpha = 30°$, 3 – $\alpha = 60°$, 4 – $\alpha = 80°$

Figure 7 – Dependence of spatial resolution of images on the distance to the image plane ($f = 50$ mm, $a = 7{,}4$ μm)

Figure 7 clearly shows that the spatial resolution of images rapidly decreases with increasing angle and not much changing with change of point coordinates x_c'. The greater the angle α, the less there is a change of spatial resolution with increasing coordinates z_C. The case of zero angle ($\alpha = 0$) indicates that the resolution remains the same for the entire image field.

2. EXPERIMENTAL INVESTIGATION OF THE INFLUENCE OF SPATIAL PARAMETERS OF THE RECEIVING SYSTEM ON IPCT MEASUREMENT RESULTS

To carry out experimental investigations of influence of the angle between the plane of the camera and the object plane on the accuracy of the results experimental setup was developed. The experimental setup is shown in Figure 8. It consists of the device 1 for shifting a background pattern (Figure 9) with the background pattern 2, the device for camera rotation 4 with respect to the plane of the background, camera 5, and 3 personal computer with installed software.

The background pattern 2 fastened to the shifting device equipped with a micrometer screw head and the indicator, which allows to control the displacement with accuracy up to 1 μm. The angle between the optical axis of the camera and the plane of the background, is controlled by a digital protractor with an accuracy up to 0,1 °. Thus, the setup created with high accuracy and repeatability for setting the parameters of the experiments. The setup used as the camera JAI RM-2040 GE, and the lens Avenir VTCH5018.

The methodology of experimental investigations is to register a series of images at different shifting of background pattern. The different series are distinguished by the angle between the optical axis of the digital camera, and the plane of the background pattern.

For each series using camera software image without shifting and with shifting horizontally from 10 to 1050 microns are captured. The experiment was carried out for several angles in the range corresponding to small angles 5°, 10°, 15° and 20°.

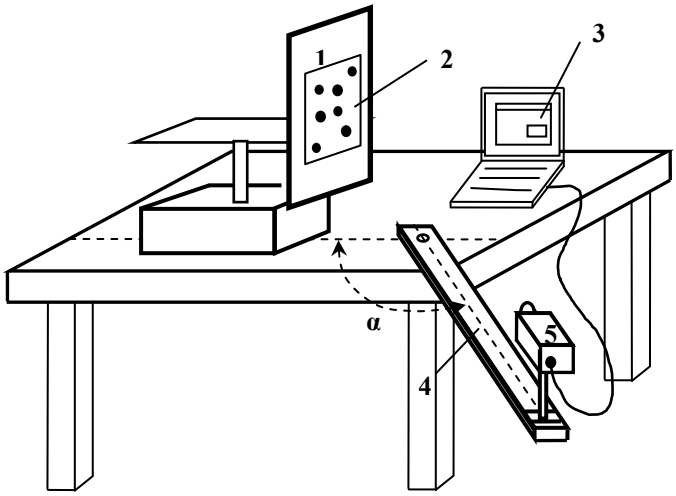

1 – the device for shifting a background pattern; 2 – background pattern; 3 – the PC; 4 – the device for camera rotation; 5 – the digital camera

Figure 8 – Scheme of experimental setup

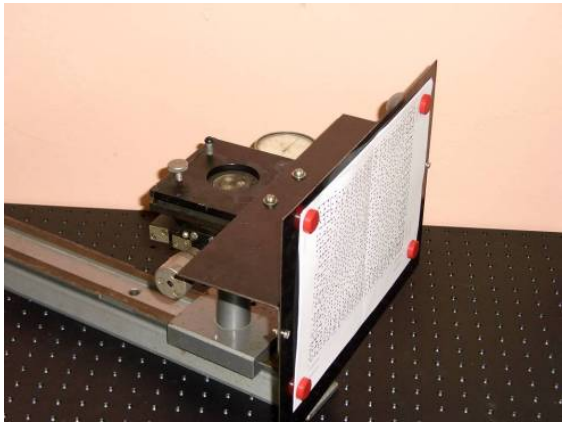

Figure 9 – Device for background pattern shifting

Studies were divided into two stages. In the first stage performed a series of experiments with 5 different background patterns presented in Figure 10.

Example of images obtained in experimental investigations shown in Figure 11. On background pattern were applied special calibration mark. The distance between them is known. Therefore, using the actual distance between the marks and the distance between them on image in pixels, calculation of the processing results in real-world units can be carried out.

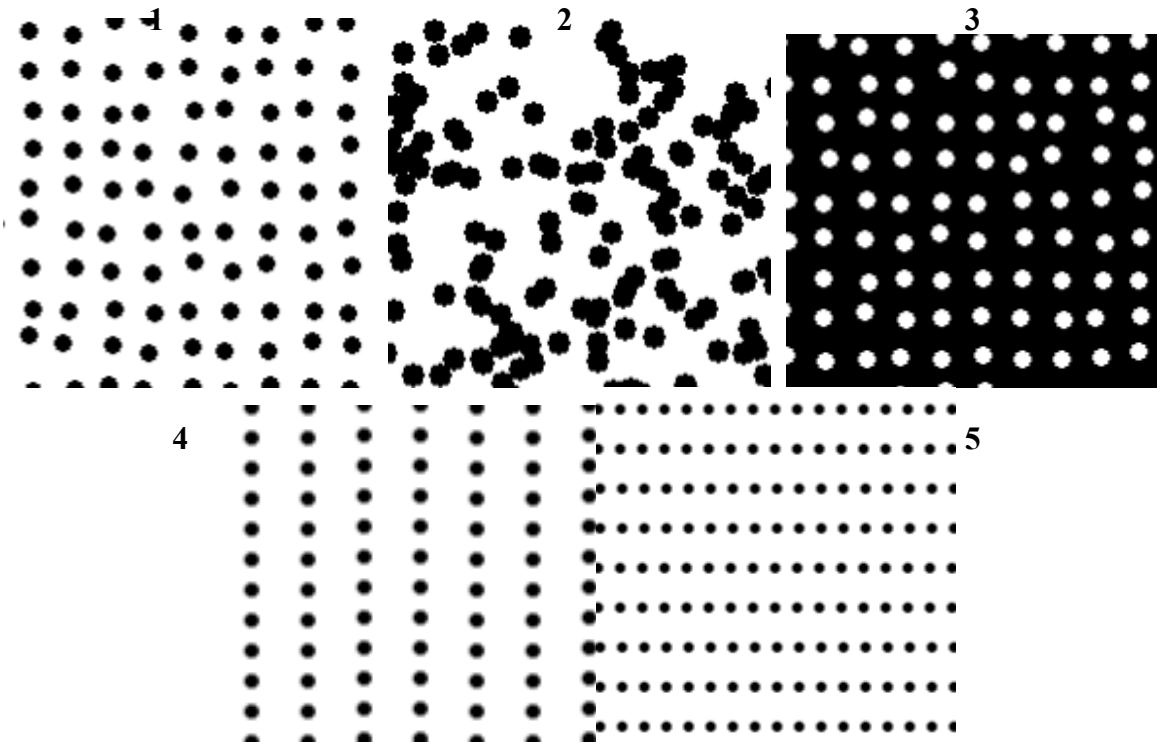

Figure 10 – Background patterns used in experimental investigations

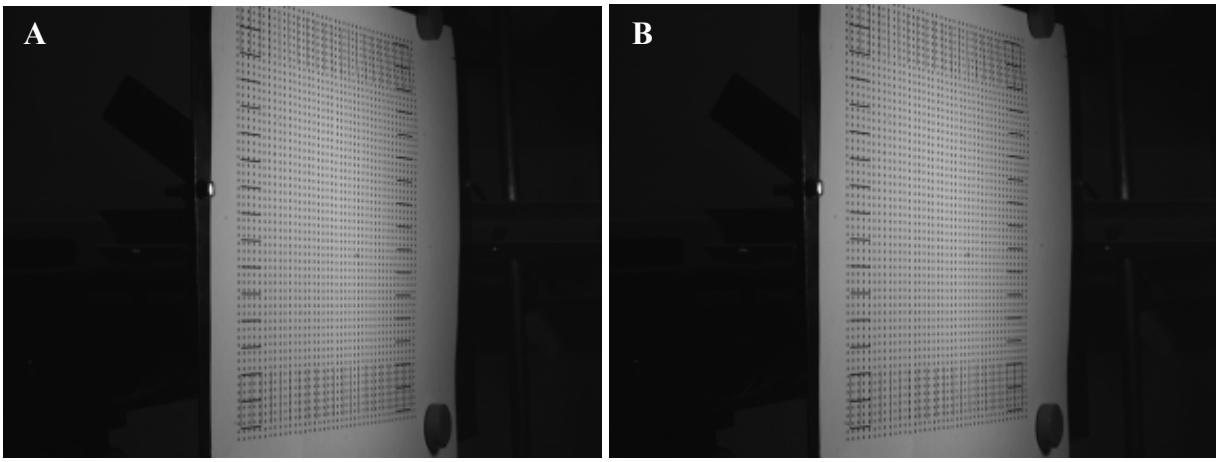

A – image without shifting, B – image with shifting on 100 μm

Figure 11 – Example of background pattern images obtained in experimental investigations

The resulting sequences of images are processed with cross correlation software. Results of processing are presented as vector field of displacement (Figure 12). The results are compared with the displacement, which was established with the help of a micrometer screw head and the indicator.

In evaluating the accuracy of the results used the relative error of the measured displacements

$$\delta d = \frac{\Delta d}{d_{tr}} \cdot 100\%, \tag{10}$$

where $\Delta d = d_{mes} - d_{tr}$, d_{tr} – true value of shifting, d_{mes} – measurement value of displacement after cross correlation processing.

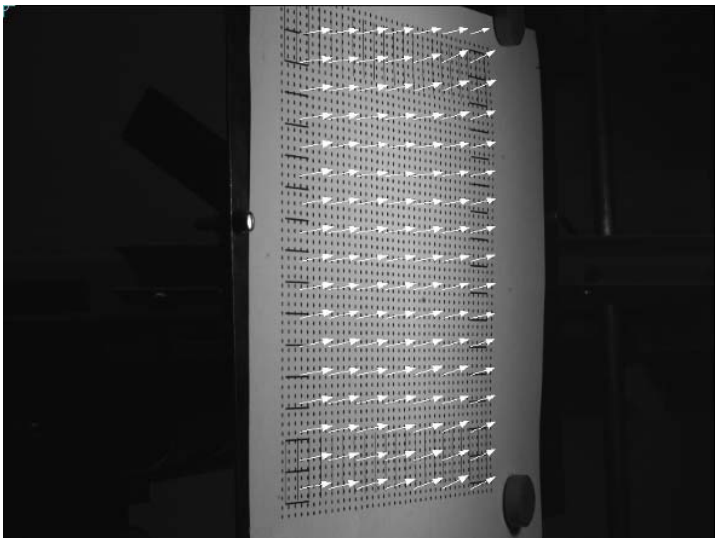

Figure 12 – Example of vector field of displacements after cross correlation processing

The results of processing experimental data for the angle between the optical axis of the camera and the plane of the background α = 5° shown in Figure 13. For small displacements from 0 to 100 microns observed variations in the relative error δd in the range from 10 to 100%. A further increase of shifting leads to stabilization of the error at 40%.

At an angle α = 10° in the displacement from 0 to 300 microns scatter in the values of error is great, but for large displacements of the relative error for the results of all the screens is reduced. At an angle α = 15° relative errors corresponding to experiments with background pattern 2, 3 and 5, in

the field of displacements from 700 to 1000 microns are reduced up to 10÷20%. The results of processing experimental data for the angle α = 20° shown in Figure 13. Dependences obtained for the results of background patterns 2, 3 and 5 are similar in nature: the error values corresponding to the shifting in the range from 700 to 1000 microns are reduced up to 10÷15%.

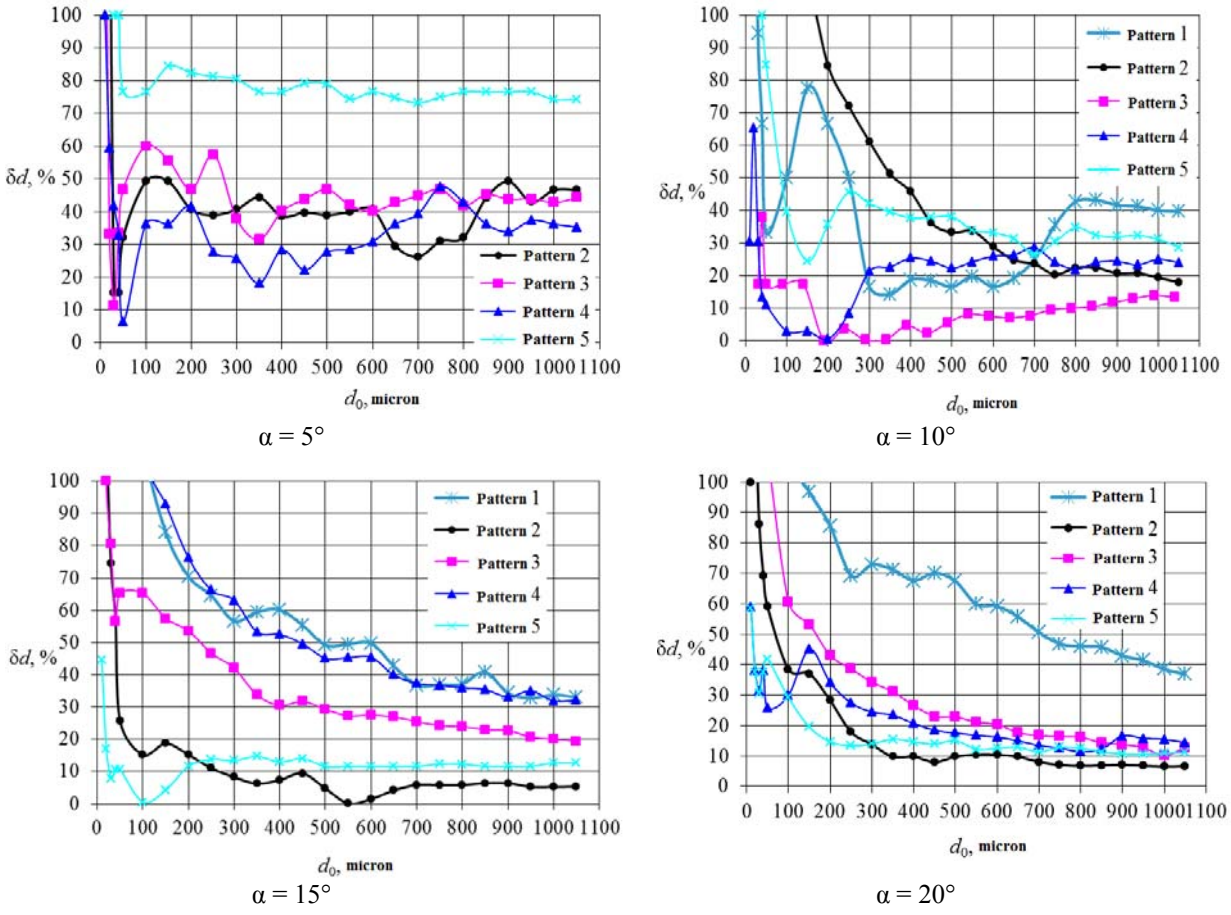

Figure 13 – Plots of the relative measurement error of the displacement δ*d* on real value of shifting for different angle of inclination

The experimental data showed that none of the five background screens yield satisfactory results for measure small shifting (up to 100 microns). And small values of the angle α between the optical axis of the camera and the plane of the background pattern results high relative error of about 40%. With increasing angle α relative error decreases. Smaller values of the error of 10÷20% were obtained at displacements from 700 to 1000 microns with background patterns 2, 3 and 5 for angles α, equal to 15° and 20°.

The second phase of the experimental investigations was carried out with the background patterns 2, 3 and 5, both showed the minimum values of the error in previous phase. To determine the stability of the obtained values of the relative error for each of the background patterns was carried out five sets of measurements for the angles α, equal to 5°, 10°, 15° and 20°.

The relative error of the results obtained with experimental data, calculated using the following formula:

$$\delta d_{\text{rnd}} = \frac{\Delta d_{\text{rnd}}}{d_{\text{avg}}} \cdot 100\%, \tag{11}$$

where Δd_{rnd} – random error of measurement in one of series; calculated with next formula

$$\Delta d_{\text{rnd}} = t_{p,n} \sqrt{\frac{\sum_{i=0}^{n} \left(\overline{d} - d_i\right)^2}{n(n-1)}}, \tag{12}$$

where $t_{p,n}$ – Student coefficient defined by two parameters (p – reliability of measurements and n – number of measurements), $\bar{d}$ – average value of measurement result, d_i – concrete measurement result. For $n = 5$ и $p = 0{,}95$ Student coefficient is equal to $t_{p,n} = 2{,}776$.

Results of second phase of experimental investigations are presented in Figure 14. The experimental results with a value of α = 5° for background pattern 3 on the whole range of displacements observed poor repeatability of results with an error of about 70%. For patterns 2 and 5 the error decreases in the range of shifting from 900 to 1000 microns and error is 20÷35%.

If the value of the angle α = 10° for patterns 2 and 5, the relative error decreases and already at shifting of 300 μm is not more than 30%. However, for the pattern 3 acceptable accuracy could not be obtained as almost all values of the error amounted to more than 50%.

If the value of the angle α = 15° results for all three patterns have good repeatability in the range of displacements from 300 to 1000 microns, where the error was no more than 25%. However, in up to 300 μm in the experiment with the pattern 3 there are two high values of the relative error of the displacement, reaching 70%. In the entire range of displacement relative error for patterns 2 and 5 did not exceed 10%, indicating a high stability of the values obtained in the processing of experimental data. Repeated series of experiments with the selected background patterns showed that the acceptable values of the random error can be achieved with a value of α = 20° with patterns 2 and 5. To obtain overall dependence of the relative error of measurements on the angle between the optical axis of the camera and the background pattern plots in Figure 15 for the pattern 5 is presented.

From Figure 15 a tendency to increase the accuracy of displacement measurements with increasing angle α can be seen. The dependence of the relative error of measurement on the angle α can be seen in Figure 16.

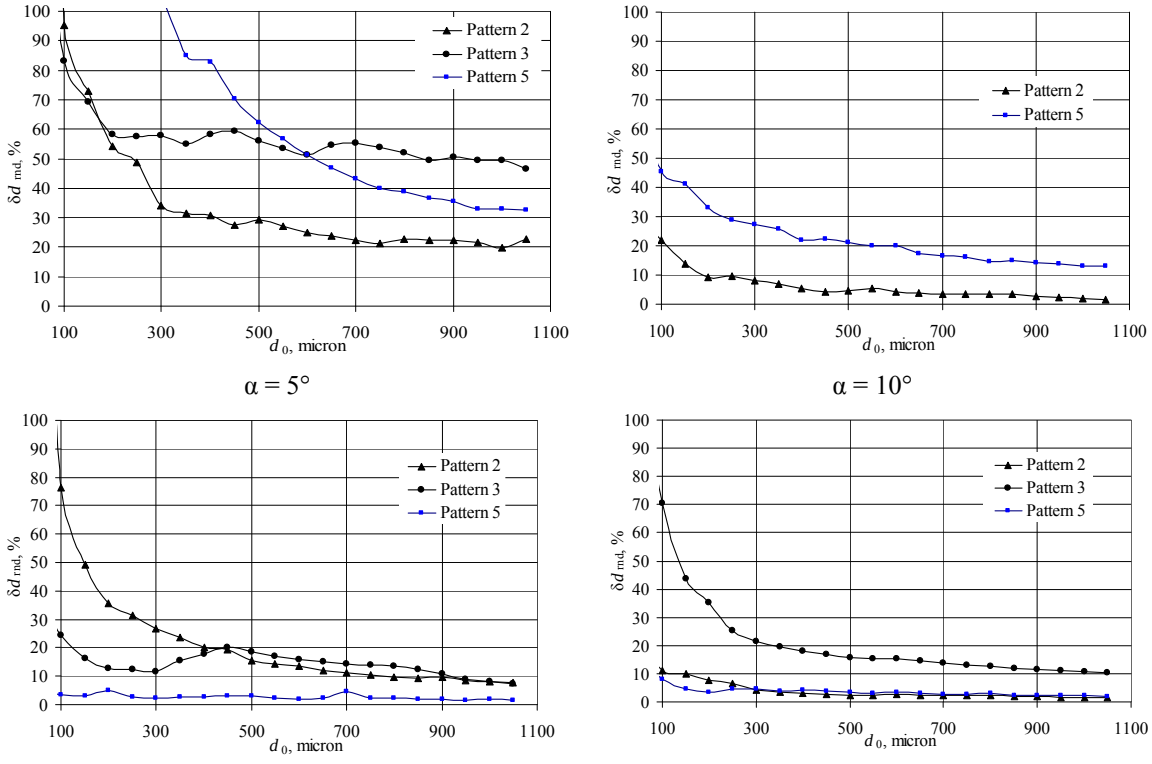

Figure 14 – Plots of the relative measurement error of the displacement δd_{rnd} on real value of shifting for different angle of inclination

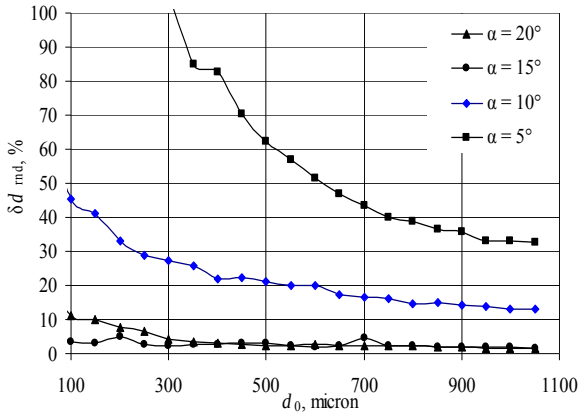

Figure 15 – Plots of the relative error of the pattern displacement δd_{rnd} on the value of real shifting at different angles α for pattern 5

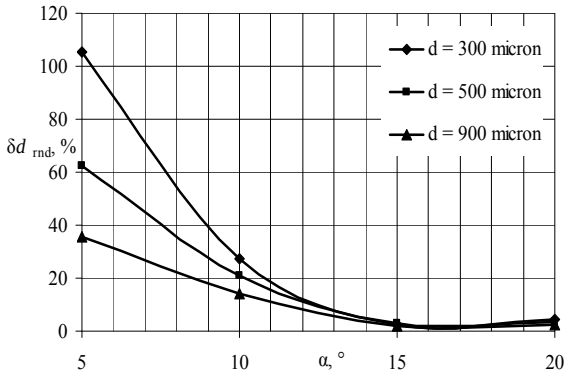

Figure 16 – Plots of the relative error of the pattern displacement δd_{rnd} on angle α for different values of the real shifting for pattern 5

The results can be explained by the following problems that were identified during the experimental investigations. The first is the lack of depth of field of the images caused by small angles between the optical axis of the camera and the plane of the background pattern, leads to a deterioration of the results of experimental data. One solution to this problem is to create an extra strong lighting and work with the minimal number of aperture, which allows to obtain a greater depth of field in images recorded by the camera even when sufficient illumination of the background pattern.

The second problem is the fact that the structure of the background screens is strongly distorted, which makes the processing of experimental data more complex. This problem can be partially solved by selecting the optimal image background pattern, which image best lends itself to further processing. However, solve it completely in with way impossible.

After experimental investigations following conclusions can be done:

- the dependences obtained show clearly that for large angles between the image plane and the investigation surface obtained images have significant non-linearity even without the aberrations;
- as the angle between the plane of the image and the investigation surface increasing the resolution of the images is a significant decrease;
- IPCT image processing techniques can not improve the spatial resolution of images obtained in experimental investigations;

As a guideline, it may be advisable in future experiments using Scheimpflug adapter, which will reduce the non-linearity and increase the spatial resolution of images obtained during the experiments.

3. INFLIGHT EXPERIMENTS [5]

Several different types of flight tests were conducted as part of the AIM project. One of the AIM subtask required the measurement of structural vibration using IPCT on small aircraft. A stereoscopic camera system has been installed to a P180 test A/C in order to check the feasibility of time resolved image based deformation measurements using IPCT for vibration testing. The comparison of deformation time series obtained from accelerometers as well as from IPCT shows that both measurements techniques give results in the same order of magnitude and with the same frequency characteristics. The remaining differences should be investigated in further studies.

The main conclusion of the presented feasibility study is, that the IPCT is a powerful easy to use tool to measure e.g. the ground shape and low frequency oscillations of a wing with a high accuracy. Limitations are given by the recordable amount of image data, the maximum camera frame

rate as well as the spatial resolution of the camera system and last but not least the optical accessibility.

After the successful application of the IPCT on the P 180 experimental test aircraft for wing vibration measurements on ground, the complete camera installation has been certified for flight testing to perform a feasibility test with in-flight IPCT for wing deformation measurements. Finally, several successful flight tests have been executed at the Piaggio Aero Industries plant in Genova (Italy).

The P180 test within the AIM project demonstrated the applicability of the IPCT for flight testing and pushes the technique toward a higher technology readiness level.

More detailed flight tests described in [5].

CONCLUTION

Computer modeling clearly shows that the spatial resolution of images rapidly decreases with increasing angle and not much changing with change of point coordinates.

After laboratory experimental investigations following conclusions can be done:

- the dependences obtained show clearly that for large angles between the image plane and the investigation surface obtained images have significant non-linearity even without the aberrations;
- as the angle between the plane of the image and the investigation surface increasing the resolution of the images is a significant decrease;
- IPCT image processing techniques can not improve the spatial resolution of images obtained in experimental investigations;

As a guideline, it may be advisable in future experiments using Scheimpflug adapter, which will reduce the non-linearity and increase the spatial resolution of images obtained during the experiments.

The P180 test within the AIM project demonstrated the applicability of the IPCT for flight testing and pushes the technique toward a higher technology readiness level.

ACKNOWLEDGEMENTS

This work was supported by the EC (7^{th} Framework Programme, project AIM^2).

REFERENCES

1. **T. Kirmse, A. Wagner** Advanced methods for in-flight flap gap and wing deformation measurements in the project AWIATOR // Proc. First CEAS Europ. Air and Space Conf. Berlin (Germany), 2007. PP. 1 – 6.

2. **C. Petit, H.W. Jentink, F. Boden, H. Kannemans, H.P.J. Veerman, T. Kirmse,** "Introducing a new measurement method for wing twist and bending", presented at ETTC 2009, Toulouse, France, 24-26 June 2009

3. **F. Boden, T. Kirmse, T. Weikert, T. Wolf, C. Petit, H.W. Jentink**, "Application of a new optical measurement technique for non-intrusive wing deformation measurements on a large transport aircraft", presented at 21st SFTE (EC) Symposium, Vergiate, AgustaWestland, paper 4, 3-6 October 2010

4. **Shapiro, Linda and George Stockman.** Computer Vision. Englewood Cliffs: Prentice Hall, 2001.

5. **Advanced In-Flight Measurement Techniques**. Eds. F. Boden, N. Lawson, H.W. Jentink, J. Kompenhans. Springer, 2013.

Лабораторные и полетные испытания МКФИ

Ф. Боден[1], А.Ю. Поройков[2], Б.С. Ринкевичюс[2], Н.М. Скорнякова[2]

[1]DLR, [2]Национальный исследовательский университет «МЭИ»

Представлены результаты теоретических исследований и лабораторного эксперимента метода корреляции фоновых изображений. Показана зависимость влияния угла наблюдения на полученные результаты. Рассмотрена возможность применения МКФИ к полетным испытаниям.

МЕТОД КОРРЕЛЯЦИИ ФОНОВЫХ ИЗОБРАЖЕНИЙ, ПОЛЕТНЫЕ ИЗМЕРЕНИЯ, ДИНАМИЧЕСКИЕ ДЕФОРМАЦИИ